of new genomic function from transposons[22–29]. We have recently shown that *Peg10* is also essential for placenta formation[18]. Although both *Rtl1* and *Peg10* are derived from the sushi-ichi–related retrotransposon, they have divergent roles, as expected from their amino acid sequences and as shown by the results of knockout experiments. *Peg10* has a DNA/RNA binding motif and an aspartyl protease motif, and it functions in placenta formation, especially in the trophoblast lineage, at an early embryonic stage. *Rtl1*, however, has only an aspartyl protease motif and functions in the maintenance of the feto-maternal interface at the late-fetal stage[16]. The important implication of these findings is that two independent exaptation events of the sushi-ichi–related retrotransposons have contributed to two different steps of placental development in the mouse.

In this work, we demonstrate that the retrotransposon-derived gene *Rtl1* is a key gene in placental development and evolution and is one of the primary genes responsible for phenotypic development in mouse PatDp(dist12)/MatDp(dist12) as well as PatDi(12)/MatDi(12). Because the remaining nine retrotransposon-derived genes also possess putative proteins, and at least some of them show expression in the placenta[16–20], identification of their origins and functions may provide important insight into placental evolution.

METHODS

Deletion of the *Rtl1* gene. Experimental procedures in this work were approved by the Animal Ethics Committees of Tokyo Medical and Dental University. We obtained 1.8-kb (nucleotides 67,582,103–67,580,338) and 7.3-kb (nucleotides 67,586,373–67,593,715) genomic DNA fragments from a mouse BAC (mRG158M19) clone containing the *Rtl1* ORF (nucleotides 67,581,614–67,586,845) and used them as the right- and left-arm sequences of a construct in which the *Rtl1* ORF was replaced with the neomycin-resistance gene. The nucleotide numbers refer to the sequence with accession number NT_039551.6. After a 2-week incubation under G418 selection, followed by electroporation of the linearized DNA into embryonic stem cells (CCE) of 129/SvEv mouse origin, we obtained 120 colonies. The genomic DNA was checked using DNA blot analysis with DNA fragments of nucleotides 67,580,998–67,581,906 and 67,607,241–67,608,065 as the 5′ and 3′ probes, respectively.

Using the *Rtl1*-targeted embryonic stem cells resulting from the homologous recombination of the construct, we made chimeric mice by blastocyst injection. Germline transmission of the knockout allele was confirmed in one male and one female chimera (*Rtl1*-LN). We carried out *in vitro* fertilization using normal C57BL/6 sperm and eggs from two *Rtl1*-LN females (indicated by the asterisks 1 and 2 in **Figure 1b** and **c**, respectively) and injected the *Cre* recombinase expression vector (pCAGGS-Cre) into the resulting fertilized eggs to produce mice that had *Rtl1*-L alleles.

All of the *Rtl1* KO lines were maintained by continuous crossing with WT B6 males and females to the F_8 generation, unless otherwise indicated.

Expression analyses of imprinted genes. Genomic DNA and total RNA were prepared from day 14.5 fetuses using ISOGEN (Nippon Gene). The methods for the quantitative RT-PCR for *Dlk1*, *Dio3*, *Meg3/Gtl2*, *Meg8/Rian* and 3′-RACE for *Rtl1* and *Rtl1as* followed by cDNA synthesis have been described previously[30]. The band intensity of *Rtl1* was measured using ImageJ software (see URLs section below).

DNA methylation analyses of IG-DMR and *Gtl2*-DMR. Purified genomic DNA was treated with sodium bisulfite solution, and the resulting DNA was amplified by the primers described previously[30]. We used the combined bisulfite restriction analysis (COBRA) method with the restriction enzyme *AciI* for IG-DMR and *TaqI* for *Gtl2*-DMR.

Placenta functional assay. We examined the efficiencies of nutrition transfer through the placenta at 15.5 d.p.c. in every fetus and placenta of the two to three litters using two radiolabeled substrates, [^{14}C]Me-AIB and [^{14}C]inulin, to measure the active and passive transport, respectively[10,11]. These substrates were dissolved in PBS and injected into the jugular vein of pregnant females. Three to four minutes after injection, the females were dissected and fetuses and placentas were sampled, because it is reported that there is minimal backflux of the radioisotopes from fetus to mother for up to 5 min[11]. The amount of the labeled substance in the fetuses and placentas was determined by a liquid scintillation counter. The counts of fetuses per milligram of placentas were calculated as the placental transfer efficiency, and the average of WT fetuses in each litter was set as 1. We compared WT and Pat-KO. Materno-fetal transfer of Me-AIB, a non-metabolizable amino acid analog usually transported across the placenta, reflects the activity of the System A amino acid transport system, whereas that of inulin reflects the passive permeability that is usually affected by the exchange barrier surface area, thickness and fetal blood flow. Using this assay, we detected only background levels of radioisotopes in the dead fetuses, whereas we found that the levels in their placentas were almost the same as that of WT and living Pat-KO placentas, providing evidence that the maternal blood flow in the placentas was still normal, even in the dead fetuses.

Histological analyses. The placentas for hematoxylin and eosin staining and IHC staining were collected and embedded in OCT compound immediately. Then, 5-μm sections were made. For hematoxylin and eosin staining, we fixed the sections in 4% paraformaldehyde (PFA) before performing the standard staining procedure. The sections were fixed in acetone for the immunostaining of CD31 and CD34, or 4% PFA for the immunostaining of Rtl1. Antibody to CD31 and antibody to CD34 (BD Pharmingen) were each used as the primary antibody, and then horseradish peroxidase (HRP)-labeled anti-rat IgG (Jackson ImmunoResearch Laboratories) was added as the secondary antibody. The antibody to Rtl1 that was produced from rabbit serum by immunizing with the synthetic Rtl1 peptide (NH_2-CGDQEAVTFRPRN-COOH) was used as the primary antibody, and then HRP-labeled anti-rabbit IgG (GE Healthcare Bio-Sciences) was added as the secondary antibody. HRP activities were visualized by diaminobenzidine (DAB) staining, and the nuclei were stained using 2% methyl green. For co-immunostaining of Rtl1 and CD31, the sections were fixed in 4% PFA. The primary antibody mixture including the antibody to CD31 and the antibody to Rtl1, and the secondary antibody mixture including the Alexa 488-conjugated anti-rat IgG (Invitrogen), Cy3-conjugated anti-rabbit IgG (Jackson ImmunoResearch Laboratories) and Hoechst 33342, were used. Images were captured and overlaid by a VB-7000 Digital Camera System (Keyence). For truidin blue staining and transmission electron microscopy, we fixed the placentas in 2.5% glutaraldehyde in 0.05 M PBS and 1% osmium tetroxide before following the standard staining methodology.

URLs. ImageJ software, http://rsb.info.nih.gov/ij/.

GenBank accession codes. The nucleotide numbers refer to the sequence of mouse chromosome 12 with accession number NT_039551.6.

Note: Supplementary information is available on the Nature Genetics website.

ACKNOWLEDGMENTS

We thank S. Aizawa of Center for Developmental Biology, RIKEN for providing the DT-A vector that was used for making *Rtl1* KO construct, E. Robertson of University of Oxford for the CCE ES cells, M. Constancia of University of Cambridge for placenta functional assay protocol, Y. Nakahara and M. Takabe of the Mitsubishi Kagaku Institute of Life Sciences for animal breeding and H. Hasegawa, N. Kawabe and A. Akatsuka of the Tokai University and S. Ichinose of the Tokyo Medical and Dental University for their assistance in immunohistochemistry and electron microscopy along with helpful discussion. This work was supported by grants from Creative Science Research, the research program of Japan Society for the Promotion of Science (JSPS), the Uehara Memorial Science Foundation, the Mitsubishi Foundation and the Ministry of Health, Labour and Welfare for Child Health and Development (17C-2) and a Grant-in-Aid for Scientific Research on Priority Areas form the Ministry of Education, Culture, Sports, Science and Technology of Japan (1508023) to F.I., the grant for young investigators from Medical Research Institute to Y.S., and the Asahi Glass Foundation and JSPS, Grants-in Aid for Scientific Research to T.K.-I. Pacific Edit reviewed the manuscript before submission.

AUTHOR CONTRIBUTIONS

Most analyses in this work were performed by Y.S. with collaboration of H.W., R.O., N.W., T.K. and M.K. in molecular and histological experiments.

Construction of *Rtl1* targeting vector was done by H.W. under supervision of K.N. and M.Y., and KO mice were produced by T.H., R.S.-M., K.N. and M.Y. The study was designed and coordinated by T.K.-I. and F.I., and the results were discussed by A.O., T.O., T.K.-I. and F.I. The paper was written by Y.S. and F.I.

Published online at http://www.nature.com/naturegenetics
Reprints and permissions information is available online at http://npg.nature.com/reprintsandpermissions

1. Rossant, J. & Cross, J.C. Placental development: lessons from mouse mutants. *Nat. Rev. Genet.* **2**, 538–548 (2001).
2. Watson, E.D. & Cross, J.C. Development of structures and transport functions in the mouse placenta. *Physiology (Bethesda)* **20**, 180–193 (2005).
3. Seitz, H. *et al.* Imprinted microRNA genes transcribed antisense to a reciprocally imprinted retrotransposon-like gene. *Nat. Genet.* **34**, 261–262 (2003).
4. Cattanach, B.M. & Rasverry, C.V. Evidence of imprinting involving the distal region of Chr 12. *Mouse Genome* **91**, 858 (1993).
5. Georgiades, P., Watkins, M., Surani, M.A. & Ferguson-Smith, A.C. Parental origin-specific developmental defects in mice with uniparental disomy for chromosome 12. *Development* **127**, 4719–4728 (2000).
6. Tevendale, M., Watkins, M., Rasberry, C., Cattanach, B. & Ferguson-Smith, A.C. Analysis of mouse conceptuses with uniparental duplication/deficiency for distal chromosome 12: comparison with chromosome 12 uniparental disomy and implications for genomic imprinting. *Cytogenet. Genome Res.* **113**, 215–222 (2006).
7. Davis, E. *et al.* RNAi-mediated allelic trans-interaction at the imprinted *Rtl1/Peg11* locus. *Curr. Biol.* **15**, 743–749 (2005).
8. Takada, S. *et al.* Epigenetic analysis of the *Dlk1-Gtl2* imprinted domain on mouse chromosome 12: implications for imprinting control from comparison with *Igf2-H19*. *Hum. Mol. Genet.* **11**, 77–86 (2002).
9. Lin, S.P. *et al.* Asymmetric regulation of imprinting on the maternal and paternal chromosomes at the *Dlk1-Gtl2* imprinted cluster on mouse chromosome 12. *Nat. Genet.* **35**, 97–102 (2003).
10. Constância, M. *et al.* Placental-specific IGF-II is a major modulator of placental and fetal growth. *Nature* **417**, 945–948 (2002).
11. Sibley, C.P. *et al.* Placental-specific insulin-like growth factor 2 (*Igf2*) regulates the diffusional exchange characteristics of the mouse placenta. *Proc. Natl. Acad. Sci. USA* **101**, 8204–8208 (2004).
12. Angiolini, E. *et al.* Regulation of placental efficiency for nutrient transport by imprinted genes. *Placenta* **27** (Suppl. A), S98–S102 (2006).
13. Moon, Y.S. *et al.* Mice lacking paternally expressed Pref-1/Dlk1 display growth retardation and accelerated adiposity. *Mol. Cell. Biol.* **22**, 5585–5592 (2002).
14. Hernandez, A., Martinez, M.E., Fiering, S., Galton, V.A. & St Germain, D. Type 3 deiodinase is critical for the maturation and function of the thyroid axis. *J. Clin. Invest.* **116**, 476–484 (2006).
15. Georgiades, P., Watkins, M., Burton, G.J. & Ferguson-Smith, A.C. Roles for genomic imprinting and the zygotic genome in placental development. *Proc. Natl. Acad. Sci. USA* **98**, 4522–4527 (2001).
16. Butler, M., Goodwin, T., Simpson, M., Singh, M. & Poulter, R. Vertebrate LTR retrotransposons of the Tf1/sushi group. *J. Mol. Evol.* **52**, 260–274 (2001).
17. Lynch, C. & Tristem, M. A co-opted gypsy-type LTR-retrotransposon is conserved in the genomes of humans, sheep, mice, and rats. *Curr. Biol.* **13**, 1518–1523 (2003).
18. Ono, R. *et al.* Deletion of *Peg10*, an imprinted gene acquired from a retrotransposon, causes early embryonic lethality. *Nat. Genet.* **38**, 101–106 (2006).
19. Brandt, J. *et al.* Transposable elements as a source of genetic innovation: expression and evolution of a family of retrotransposon-derived neogenes in mammals. *Gene* **345**, 101–111 (2005).
20. Youngson, N.A., Kocialkowski, S., Peel, N. & Ferguson-Smith, A.C. A small family of sushi-class retrotransposon-derived genes in mammals and their relation to genomic imprinting. *J. Mol. Evol.* **61**, 481–490 (2005).
21. Kagami, M. *et al.* Deletions and epimutations affecting the human 14q32.2 imprinted region in individuals with paternal and maternal upd(14)-like phenotypes. *Nat. Genet.* advance online publication, doi:10.1038/ng.2007.56 (6 January 2008).
22. Gould, S. & Vrba, S. Exaptation—a missing term in the science of form. *Paleobiology* **8**, 4–15 (1982).
23. Brosius, J. & Gould, S.J. On "genomenclature": a comprehensive (and respectful) taxonomy for pseudogenes and other "junk DNA". *Proc. Natl. Acad. Sci. USA* **89**, 10706–10710 (1992).
24. Smit, A.F. Interspersed repeats and other mementos of transposable elements in mammalian genomes. *Curr. Opin. Genet. Dev.* **9**, 657–663 (1999).
25. Mi, S. *et al.* Syncytin is a captive retroviral envelope protein involved in human placental morphogenesis. *Nature* **403**, 785–789 (2000).
26. Kazazian, H.H., Jr. Mobile elements: drivers of genome evolution. *Science* **303**, 1626–1632 (2004).
27. Dupressoir, A. *et al.* Syncytin-A and syncytin-B, two fusogenic placenta-specific murine envelope genes of retroviral origin conserved in Muridae. *Proc. Natl. Acad. Sci. USA* **102**, 725–730 (2005).
28. Bejerano, G. *et al.* A distal enhancer and an ultraconserved exon are derived from a novel retroposon. *Nature* **441**, 87–90 (2006).
29. Biémont, C. & Vieira, C. Genetics: junk DNA as an evolutionary force. *Nature* **443**, 521–524 (2006).
30. Sekita, Y. *et al.* Aberrant regulation of imprinted gene expression in *Gtl2*^{lacZ} mice. *Cytogenet. Genome Res.* **113**, 223–229 (2006).

Clin Pediatr Endocrinol 2007; **16**(4), 85-87

Original Article

Target Height and Target Range for Japanese Children: Revisited

Tsutomu Ogata[1], Toshiaki Tanaka[2], Masayo Kagami[1]

[1]*Department of Endocrinology and Metabolism, National Research Institute for Child Health and Development, Tokyo, Japan*

[2]*Department of Laboratory Medicine, National Center for Child Health and Development, Tokyo, Japan*

Abstract. In 1990, we proposed the equations to calculate target height (TH) and target range (TR) for Japanese, taking account of the positive height secular trend observed over the last ~100 years. However, height difference between generations appears to have become small or negligible in contemporary Japanese populations. Thus, we re-analyzed the Japanese height data, and revised the equations for TH and TR for contemporary Japanese children as follows (cm): Boys, TH = {PH + (MH + 13)} ÷ 2, TR = TH ± 9; and Girls, TH = {(PH − 13) + MH} ÷ 2; TR = TH ± 8, where PH indicates paternal height and MH maternal height.

Key words: target height, target range, Japanese

Introduction

Height is a quantitative character subject to various genetic and environmental factors (1). In developed countries, including Japan, genetic factors have become the major height determinants, because environmental factors have generally improved to a high degree with few gross variations among individuals. Indeed, heredity, which is defined as the relative contribution of genetic factors to the determination of individual height, is regarded as contributing 80–90% to height in developed countries (2). In this context, parental height can be regarded as an excellent indication for the genetic factors, because the heights of children correlate well with their parental heights (3).

Tanner *et al.* proposed the concept of target height (TH) and target range (TR), which predict the adult height and its range of variation on the basis of parental height (3). In 1990, Ogata *et al.* proposed the following equations to calculate TH/TR for Japanese (cm): boys, TH = {PH + (MH + 13)} ÷ 2 + 2, TR = TH ± 9; and girls, TH = {(PH − 13) + MH} ÷ 2 + 2; TR = TH ± 8, where PH indicates paternal height and MH maternal height (4). In these equations, the "2 cm" represents the height difference between generations that has primarily been caused by improvement in environmental factors over the last ~100 years. However, as indicated by the recent cessation of the positive height secular trend, the height difference between generations appears to have become small or negligible in contemporary Japanese populations.

Received: May 30, 2007
Accepted: July 23, 2007
Correspondence: Dr. Tsutomu Ogata, Department of Endocrinology and Metabolism, National Research Institute for Child Health and Development, 2-10-1 Ohkura, Setagaya, Tokyo 157-8535, Japan
E-mail: tomogata@nch.go.jp

Thus, we re-analyzed growth parameters utilized in the calculation of TH/TR, and set forth revised equations for the calculation of TH/TR. We further discuss several points regarding the clinical application of TH/TR.

Methods

Theoretically, TH/TR (cm) is obtained by the following equations (3).

Boys: $TH = \{PH + (MH + D)\} \div 2 + d_1$; $TR = TH \pm 2RSD_1 = TH \pm 2SD_1 \div \sqrt{1 - r^2}$.

Girls: $TH = \{(PH - D) + MH\} \div 2 + d_2$; $TR = TH \pm 2RSD_2 = TH \pm 2SD_2 \div \sqrt{1 - r^2}$.

D: adult height difference between sexes; d_1: adult height difference between male generations; d_2: adult height difference between female generations; RSD: residual standard deviation; SD_1: adult height standard deviation in males; SD_2: adult height standard deviation in females; and r: correlation coefficient between mid-parental height and child's adult height.

To determine the variables utilized in the equations for TH/TR (D, d_1, d_2, SD_1, and SD_2), we examined the heights at 17.5 yr of age on the basis of the annual data from the Ministry of Education, Culture, Sports, Science and Technology, because there are no reliable adult height data in Japan. Furthermore, since there are no data of r, we employed the practical value of 0.63 that is obtained by reducing the relevance of assortative mating and other factors from the theoretical value of 0.71 that is obtained by assuming random mating (3). The generation time was evaluated as roughly 30 yr on the basis of the parental age data at the birth of children from the Ministry of Health, Labour and Welfare; this implies that the secular trend since 1985 is important in the assessment of d_1 and d_2 for contemporary Japanese children ~6 years of age at present (the year 2007), because their parents are predicted to have reached the adult height around the year 1988 (at ~17.5 years of age) and produced children around the year 2001 (at ~30 years of age).

Table 1 Height data at 17.5 yr of age (cm)

Year	Boys		Girls		D
	Height	SD	Height	SD	
1985	170.2	5.60	157.6	4.98	12.6
1986	170.3	5.64	157.7	4.99	12.6
1987	170.3	5.71	157.8	4.97	12.5
1988	170.3	5.65	157.8	5.05	12.5
1989	170.5	5.63	157.8	5.00	12.7
1990	170.4	5.57	157.9	4.99	12.5
1991	170.6	5.62	157.9	5.04	12.7
1992	170.7	5.65	157.9	5.14	12.8
1993	170.7	5.61	158.0	5.19	12.7
1994	170.9	5.68	158.1	5.20	12.8
1995	170.8	5.64	158.0	5.17	12.8
1996	170.9	5.74	158.1	5.23	12.8
1997	170.9	5.76	158.0	5.26	12.8
1998	170.9	5.81	158.1	5.22	12.8
1999	170.9	5.80	158.1	5.22	12.8
2000	170.8	5.83	158.1	5.25	12.7
2001	170.9	5.76	158.0	5.32	12.9
2002	170.7	5.72	157.9	5.26	12.8
2003	170.7	5.72	157.8	5.29	12.9
2004	170.8	5.83	157.9	5.35	12.9
2005	170.8	5.81	158.0	5.28	12.8

SD: standard deviation; D: sex difference in height.

Results

The height data at 17.5 yr of age from the year 1985 to 2005 is shown in Table 1. The height difference between sexes remained constant with a range of 12.5–12.9 cm. The height at 17.5 yr of age also remained fairly constant and, virtually, there was no height change for >10 yr in boys and >15 yr in girls. The height SD also remained constant with a range of 5.60–5.83 cm in boys and 4.97–5.35 cm in girls. Thus, considering the clinical convenience, we determined the "D" as 13.0 cm (the height gain after 17.5 yr of age should be slightly larger in boys than in girls), the "d_1" and "d_2" values as zero, RSD_1 as 4.5 cm, and RSD_2 as 4.0 cm (SD_1 and SD_2 were obtained as 5.71 cm and 5.20 cm based on the median values, and r was regarded as 0.63). Thus, we set forth the

following equations for contemporary Japanese children:

Boys, TH = {PH + (MH + 13)} ÷ 2 cm; TR = TH ± 9 cm

Girls, TH = {(PH − 13) + MH} ÷ 2 cm; TR = TH ± 8 cm.

Discussion

We re-analyzed the annual height data in Japan, and confirmed virtually no secular height change in recent decades in both sexes. Thus, there appears to be no need to take account of the adult height difference between generations in both boys and girls. Furthermore, we also confirmed that there is no need to change other parameters utilized in the TH/TR equations. On the basis of these findings, we have revised the TH/TR equations for contemporary Japanese children.

While the usefulness of TH/TR has widely been accepted, several matters should be considered in the clinical application of TH/TR (5). First, TH/TR cannot be utilized for a child born to a parent(s) with a mutant major growth gene. For example, it does not make sense at all to use TH/TR in the height assessment of a child born to a father with achondroplasia and a normal mother. Second, there should be no drastic difference in the environmental factors between the two generations. Drastic changes in environmental factors have taken place after the World War II (4), and environmental factors could change drastically in several situations such as neglect. Third, since only mean values are utilized for the equations of TH/TR, the accuracy should be different depending on the parental height. For example, although TH/TR is similar between a child born to parents of average height and a child born to a tall father and a short mother, the height variation must be larger in the latter child than in the former child. Fourth, if the child's height remains within the TR, this does not guarantee that the child has no abnormality of a major growth gene. For example, haploinsufficiency of *SHOX* is known to reduce the statural height by ~2 SD in patients without dyschondrosteosis (6). Thus, a person with a high original height potential, e.g., the upper limit of TR, can still have a height within the TR under haploinsufficiency of *SHOX*. Lastly, if the child's height is outside the TR, this does not necessarily indicate that the child has an abnormality of a major growth gene. Tall stature above TR and short stature below TR can take place just by chance with the frequency of 2.3%.

In summary, we set forth the TH/TR equations for contemporary Japanese children. It is recommended to use TH/TR in the growth assessment of children, taking account of its limitations.

Acknowledgement

This study was supported by a grant for Child Health and Development from the Ministry of Health, Labour, and Welfare (17C-2).

References

1. Vogel F, Motulsky AG. Human Genetics: Problems and Approaches. Springer-Verlag, Berlin/ Heidelberg/New York/Tokyo, 1986.
2. Silventoinen K, Kaprio J, Lahelma E, Koskenvuo M. Relative effect of genetic and environmental factors on body height: differences across birth cohorts among Finnish men and women. Am J Public Health 2000;90:627–30.
3. Tanner JM. Use and abuse of growth standards. In: Falkner F, Tanner JM, editors. Human growth 2nd ed, Vol. 3. Plenum, New York/London, 1986: p.95–109.
4. Ogata T, Matsuo N, Tamai S, Osano M, Tango T. Target height and target range for the Japanese. Jpn J Paediatr 1990; 94:1535–40 (in Japanese).
5. Ogata T. Genetics of human growth. Clin Pediatr Endocrinol 2006;15:45–53.
6. Ogata T. SHOX haploinsufficiency: lessons from clinical studies. Cur Opin Endocrinol Diabetes 2002;9:13–20.

doi:10.1111/j.1741-4520.2006.00140.x

CASE REPORT

EFNB1 mutation at the ephrin ligand-receptor dimerization interface in a patient with craniofrontonasal syndrome

Chiharu Torii[1]*, Kosuke Izumi[1]*, Hideo Nakajima[2], Takao Takahashi[1], and Kenjiro Kosaki[1]

Departments of [1]Pediatrics and [2]Plastic and Reconstructive Surgery, Keio University School of Medicine, Tokyo, Japan

ABSTRACT **Craniofrontonasal syndrome (CFNS) is characterized by craniosynostosis, hypertelorism, a broad nasal tip and occasionally cleft lip and palate, and is caused by a mutation in the *ephrin-B1* gene (*EFNB1*). The study of naturally occurring human *EFNB1* mutations offers a unique opportunity to better define the critical portion within the ephrin domain that is essential for the function of EFNB1 protein in craniofacial development. Here, we report a CFNS patient with a novel *EFNB1* missense mutation present at the interface between EFNB1 and its receptor proteins. The patient's facial features included hypertelorism, a broad nasal tip, brachycephaly, frontal bossing, facial asymmetry and esotropia. In addition, she had pectus carinatum, grooved nails on her thumb, an abnormal palmar crease pattern and a broad first toe. Her development was appropriate for her age. Direct sequencing of polymerase chain reaction products using an autosequencer revealed a heterozygous missense mutation, Ser118Ile. Ser118 is located in the G-H loop of the extracellular ephrin domain and is highly evolutionarily conserved among rodents, avians and fish. The mutation occurred *de novo* and was not present in 100 normal Japanese control subjects. Substitutions of the adjacent amino acid residue, Pro119, have been previously reported in three CFNS patients. Since the structure of EFNB1 is not yet available, the spatial locality of Ser118 was characterized using the protein structure of EFNB2. We deduced that Ser118 in EFNB1 resides at the major dimerization interface with Eph receptors and inferred that the Ser118Ile mutation may impede the protrusion of the G-H loop, thereby disturbing Eph–Ephrin signal transduction.**

Key Words: craniosynostosis, mutation analysis, ephrin, Eph

INTRODUCTION

Craniofrontonasal syndrome (CFNS[MIM 304110]) is characterized by hypertelorism, a widow's peak, a broad nasal tip and, occasionally, cleft lip and palate (Cohen 1979; Slover & Sujansky 1979). Craniofacial asymmetry is often apparent because of unilateral coronal synostosis. Extracranial manifestations include thoracic deformity, polydactyly, grooved nails and clinodactyly of the fifth finger. Developmental delay is not usually present. The CFNS trait is transmitted vertically with no male-to-male transmission, a pattern suggestive of X-linked inheritance. However, the inheritance pattern of the CFNS phenotype is unique in that female patients are more severely affected than male patients (Saavedra *et al.* 1996; Wieacker & Wieland 2005). X-linked inheritance was confirmed by a mapping study conducted by Wieland *et al.* and the *ephrin-B1* gene (*EFNB1*) was identified as the causative gene for CFNS (Wieland *et al.* 2002, 2004; Twigg *et al.* 2004).

EFNB1 is a member of the ephrin ligand family of proteins, which consists of membrane-anchored ligands for Eph receptor tyrosine kinases (Beckmann *et al.* 1994). There are two structural classes of ephrin ligand proteins. Ephrin-A proteins (EFNA1, EFNA2, EFNA3, EFNA4 and EFNA5) are anchored through the attachment of a glycosylphosphatidylinositol group to their C-terminal region, whereas ephrin-B proteins (EFNB1, EFNB2 and EFNB3) have a transmembrane and cytoplasmic domain. The receptors for ephrin-A and ephrin-B proteins are EphA proteins (EphA1-8) and EphB proteins (EphB1-4, EphB6), respectively. Eph/ephrin signaling is an essential developmental regulatory pathway in diverse biological processes, including development, tissue patterning and angiogenesis (Klein 2004; Poliakov *et al.* 2004; Surawska *et al.* 2004; Martinez & Soriano 2005; Pasquale 2005).

Among previous reports analyzing *EFNB1* mutations, 87 out of 101 cases (86%) were revealed to have *EFNB1* mutations. The mutation classes among these 87 cases included whole gene deletions (3 cases), intragenic deletions (2 cases), frameshift mutations (24 cases), nonsense mutations (13 cases), missense mutations (39 cases) and splice site mutations (6 cases) (Twigg *et al.* 2004, 2006; Wieland *et al.* 2004, 2005; Shotelersuk *et al.* 2006). The majority of the missense mutations were located in exons 2 and 3 of the *EFNB1* gene, which encode the extracellular ephrin domain (ephrin domain). The study of naturally occurring human *EFNB1* mutations offers a unique opportunity to better define the critical portion within the ephrin domain that is essential for the function of EFNB1 protein in craniofacial development. Here, we report a CFNS patient with a novel *EFNB1* Ser to Ile missense mutation present at the interface between EFNB1 and its receptor proteins.

CASE REPORT

A Japanese girl was born at 38 weeks of gestation by vaginal delivery. The parents were non-consanguineous and phenotypically normal. Fetal ultrasonography performed during the nineteenth week of pregnancy revealed cranial deformity. The patient's birth weight was 3002 g (25–50th percentile), her length was 48.0 cm (25–50th percentile), and her occipitofrontal circumference was 35.0 cm (90–97th percentile). Her Apgar scores were 8 at 1 min and 9 at 5 min. Cranial deformity was apparent during the neonatal period and a computed tomography scan demonstrated a premature fusion of the right coronal suture, with no structural abnormalities in the brain. The patient's chromosomes were normal.

At the age of 8 months her weight was 7.1 kg (10–25th percentile), her length was 70.7 cm (75–90th percentile) and her occipitofrontal circumference was 42.0 cm (10–25th percentile).

Correspondence: Kenjiro Kosaki, MD, Division of Medical Genetics, Department of Pediatrics, Keio University School of Medicine, 35 Shinanomachi, Shinjuku-ku, Tokyo 160-8582, Japan. Email: kkosaki@sc.itc.keio.ac.jp

*These authors contributed equally to this work.

Received July 4, 2006; revised and accepted September 6, 2006.

Her facial features included hypertelorism, a broad nasal tip, brachycephaly, frontal bossing, facial asymmetry and strabismus (esotropia; Fig. 1). In addition, she had pectus carinatum, grooved nails on her thumb, an abnormal palmar crease pattern, and a broad first toe. Her development was appropriate for her age. She could stand with holding, crawled freely, exhibited a fine pincer grasp and played pat-a-cake. She was diagnosed as having CFNS. After obtaining informed consent from her parents, we screened the patient for *EFNB1* mutation.

MOLECULAR STUDIES

The coding exons of the human *EFNB1* gene were screened for mutations using polymerase chain reaction (PCR) analysis. The genomic DNA was amplified by PCR using primers, the design of which was based on published genomic sequences (GenBank accession numbers AL136092 for *EFNB1*). The primer sequences and PCR conditions are available on request. Direct sequencing of the PCR products using an autosequencer (ABI3100, ABI, Foster City, CA, USA) revealed a heterozygous 353 G > T transition leading to a missense mutation, Ser118Ile. Ser118 is located in the extracellular ephrin domain and is highly evolutionarily conserved among rodents, avians and fish (Fig. 2). The mutation was not present in 100 normal Japanese control subjects or the parents.

To characterize the spatial locality of the substituted amino acid, the protein structure of EFNB2 was visualized using the WebMol viewer in the Research Collaboratory for Structural Bioinformatics (RCSB) protein databank (http://www.rcsb.org/pdb/Welcome.do). Because the crystal structure of ephrin-B1 is not yet available, we used the ephrin-B2 structure instead. We believe the substitution of the EFNB2 structure was legitimate because EFNB1 and EFNB2

Fig. 1 Facial features of the patient at 10 months of age. Hypertelorism, a broad nasal tip, brachycephaly, frontal bossing, facial asymmetry and esotropia were present.

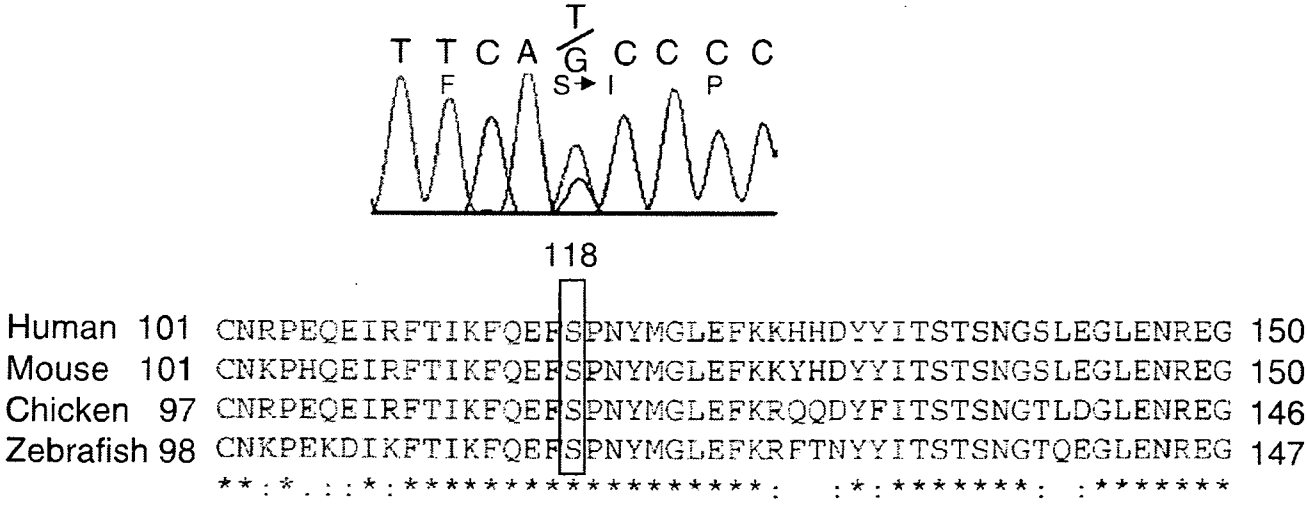

Fig. 2 Identification of the *EFNB1* mutation. Top: Sequence chromatogram of the patient. Bottom: Evolutionary conservation of the substituted amino acid residue in humans, mice, chickens and zebrafish.

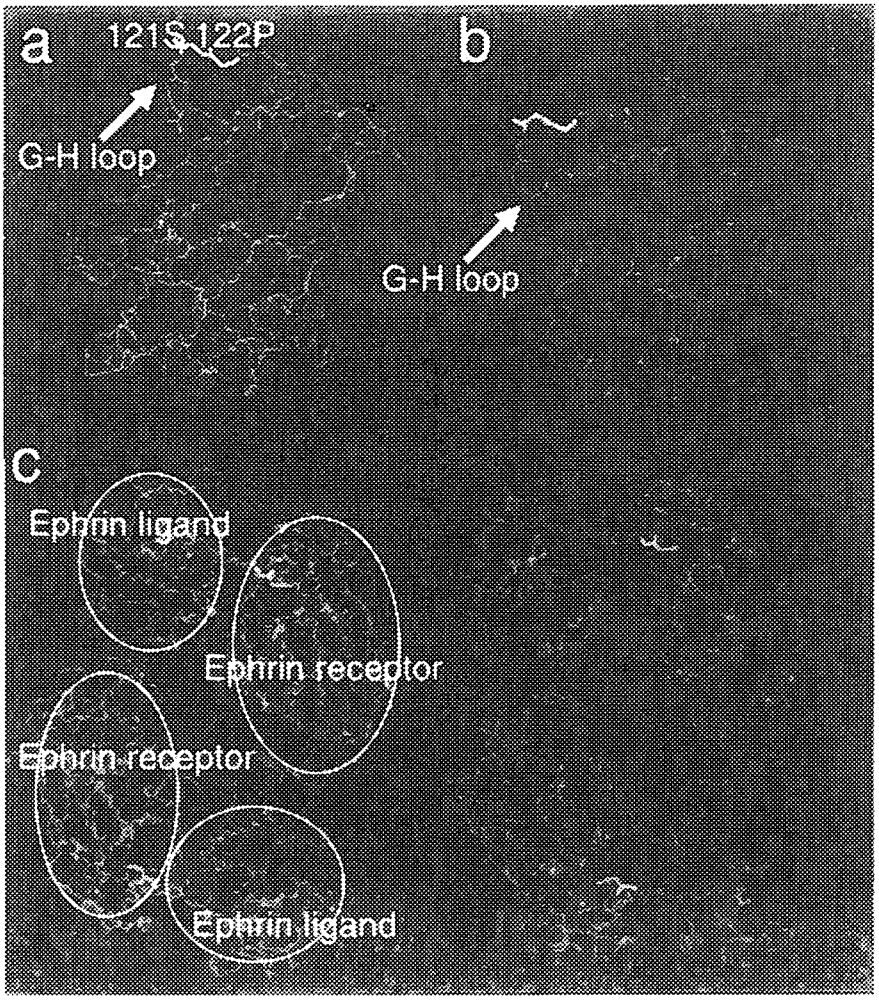

Fig. 3 Three-dimensional view of the substituted amino acid residue's location. The data were obtained from the RCSB protein databank and the rotated images were generated using the WebMol viewer. Yellow: location of the S121 residue that was substituted in the present patient. Pink: location of the P122 residues that were substituted in a previously reported mutation analysis series. (a) Crystal structure of the murine Efnb2 ectodomain. (b) Crystal structure of the murine Efnb2 ectodomain, viewed from a different angle than that in (a). (c) Crystal structure of the Ephb2 (receptor)-Efnb2 (ligand) tetrad complex. The left and right images are identical, except for the annotations on the left image.

have a high degree of sequence homology (43% amino acid identity) and a similar overall structure and binding affinity to EphB2 (Nikolov *et al.* 2005). Using the crystal structure of the mouse Ephb2-Efnb2 complex tetramer, we localized the substituted serine residue (Fig. 3) (Himanen *et al.* 2001; Toth *et al.* 2001). Ser118 was predicted to interact with the Eph receptor at the major dimerization interface.

DISCUSSION

We identified a novel *de novo EFNB1* missense mutation, Ser118Ile, located at the surface of the ephrin ligand–Eph receptor interaction site in a patient with CFNS. The high degree of conservation of the Ser118 residue in an evolutionary context, as well as its conservation among ephrin-B proteins, indicates a functional significance. Substitutions of the adjacent amino acid residue, Pro119, have been previously reported in three CFNS patients (Pro119Ser, Pro119His and Pro119Ala) (Twigg *et al.* 2004, 2006). Ser118 and Pro119 reside in a stretch of 11 conserved amino acids (Q115-E125) that is referred to as the G-H loop (Toth *et al.* 2001). Together with the three patients with Pro119 mutations, the documentation of the present CFNS patient with a Ser118 substitution lends further support to the notion that the GH-loop is functionally important.

Ephrins, including EFNB1, form heterodimers with Eph receptors, and two Eph-ephrin dimers then form a tetramer. *In vitro* studies have indicated that the protrusion of the G-H loop of ephrin into the Eph receptor represents the critical step in the Eph-ephrin dimerization process (Himanen *et al.* 2001). A structural analysis indicated that the Ser118 and Pro119 residues are located at the tip of the G-H loop. We suspect that amino acid substitutions at Ser 118 or Pro119 may impede the protrusion of the G-H loop, disturbing Eph-Ephrin signal transduction.

Recently, heterozygous mutations in *EFNA4* were shown to cause non-syndromic coronal synostosis. Although patients with *EFNA4* mutations do not have hypertelorism and thus do not have the CFNS phenotype, it is interesting to note that patients with *EFNB1* mutations and those with *EFNA4* mutations both exhibit coronal craniosynostosis. Furthermore, one of these *EFNA4* mutations was located in a region equivalent to the highly conserved G-H loop amino acids (Q115-E125) of ephrin-B1, suggesting that this region plays a critical role not only in EFNB1, but also in other members of the ephrin protein family and in the propagation of ephrin-Eph signaling (Merrill *et al.* 2006).

ACKNOWLEDGMENTS

This research was partially supported by a Grant-in-Aid from the Japanese Ministry of Education, Culture, Sports, Science and Technology, and the Ministry of Health, Labor and Welfare.

REFERENCES

Beckmann MP, Cerretti DP, Baum P *et al.* (1994) Molecular characterization of a family of ligands for eph-related tyrosine kinase receptors. *EMBO J* **13**: 3757–3762.

Cohen MM Jr (1979) Craniofrontonasal dysplasia. *Birth Defects Orig Artic Ser* **15**: 85–89.

Himanen JP, Rajashankar KR, Lackmann M, Cowan CA, Henkemeyer M, Nikolov DB (2001) Crystal structure of an eph receptor-ephrin complex. *Nature* **414**: 933–938.

Klein R (2004) Eph/ephrin signaling in morphogenesis, neural development and plasticity. *Curr Opin Cell Biol* **16**: 580–589.

Martinez A, Soriano E (2005) Functions of ephrin/eph interactions in the development of the nervous system: Emphasis on the hippocampal system. *Brain Res Brain Res Rev* **49**: 211–226.

Merrill AE, Bochukova EG, Brugger SM *et al.* (2006) Cell mixing at a neural crest–mesoderm boundary and deficient ephrin-eph signaling in the pathogenesis of craniosynostosis. *Hum Mol Genet* **15**: 1319–1328.

Nikolov DB, Li C, Barton WA, Himanen JP (2005) Crystal structure of the ephrin-B1 ectodomain: Implications for receptor recognition and signaling. *Biochemistry* **44**: 10947–10953.

Pasquale EB (2005) Eph receptor signalling casts a wide net on cell behaviour. *Nat Rev Mol Cell Biol* **6**: 462–475.

Poliakov A, Cotrina M, Wilkinson DG (2004) Diverse roles of eph receptors and ephrins in the regulation of cell migration and tissue assembly. *Dev Cell* **7**: 465–480.

Saavedra D, Richieri-Costa A, Guion-Almeida ML, Cohen MM Jr (1996) Craniofrontonasal syndrome: Study of 41 patients. *Am J Med Genet* **61**: 147–151.

Shotelersuk V, Siriwan P, Ausavarat S (2006) A novel mutation in EFNB1, probably with a dominant negative effect, underlying craniofrontonasal syndrome. *Cleft Palate Craniofac J* **43**: 152–154.

Slover R, Sujansky E (1979) Frontonasal dysplasia with coronal craniosynostosis in three sibs. *Birth Defects Orig Artic Ser* **15**: 75–83.

Surawska H, Ma PC, Salgia R (2004) The role of ephrins and eph receptors in cancer. *Cytokine Growth Factor Rev* **15**: 419–433.

Toth J, Cutforth T, Gelinas AD, Bethoney KA, Bard J, Harrison CJ (2001) Crystal structure of an ephrin ectodomain. *Dev Cell* **1**: 83–92.

Twigg SR, Kan R, Babbs C *et al.* (2004) Mutations of ephrin-B1 (EFNB1), a marker of tissue boundary formation, cause craniofrontonasal syndrome. *Proc Natl Acad Sci USA* **101**: 8652–8657.

Twigg SR, Matsumoto K, Kidd AM *et al.* (2006) The origin of EFNB1 mutations in craniofrontonasal syndrome: Frequent somatic mosaicism and explanation of the paucity of carrier males. *Am J Hum Genet* **78**: 999–1010.

Wieacker P, Wieland I (2005) Clinical and genetic aspects of craniofrontonasal syndrome: Towards resolving a genetic paradox. *Mol Genet Metab* **86**: 110–116.

Wieland I, Jakubiczka S, Muschke P *et al.* (2002) Mapping of a further locus for X-linked craniofrontonasal syndrome. *Cytogenet Genome Res* **99**: 285–288.

Wieland I, Jakubiczka S, Muschke P *et al.* (2004) Mutations of the ephrin-B1 gene cause craniofrontonasal syndrome. *Am J Hum Genet* **74**: 1209–1215.

Wieland I, Reardon W, Jakubiczka S *et al.* (2005) Twenty-six novel EFNB1 mutations in familial and sporadic craniofrontonasal syndrome (CFNS). *Hum Mutat* **26**: 113–118.

American Journal of Medical Genetics Part A 143A:721–726 (2007)

Clinical Report

An *Alu* Retrotransposition-Mediated Deletion of *CHD7* in a Patient With CHARGE Syndrome

Toru Udaka,[1] Nobuhiko Okamoto,[2] Michihiko Aramaki,[1] Chiharu Torii,[1] Rika Kosaki,[3] Noboru Hosokai,[4] Toshiyuki Hayakawa,[5] Naoyuki Takahata,[6] Takao Takahashi,[1] and Kenjiro Kosaki[1]*

[1]Department of Pediatrics, Keio University School of Medicine, Tokyo, Japan
[2]Department of Planning and Research, Osaka Medical Center and Research Institute for Maternal and Child Health, Osaka, Japan
[3]Department of Clinical Genetics and Molecular Medicine, National Children's Medical Center, Tokyo, Japan
[4]Research and Development Division, Mitsubishi Kagaku Bio-Clinical Laboratory, Tokyo, Japan
[5]Department of Infectious Disease Control, International Research Center for Infectious Diseases, Research Institute for Microbial Diseases, Osaka University, Suita, Japan
[6]Department of Biosystems Science, Graduate University for Advanced Studies, Hayama, Kanagawa, Japan

Received 13 January 2006; Accepted 17 July 2006

CHD7 mutations account for about 60–65% among more than 200 CHARGE syndrome cases. When rare whole gene deletion cases associated with chromosomal abnormalities are excluded, all mutations of *CHD7* reported to date have been point mutations and small deletions and insertions, rather than exonic deletions. To test whether exonic deletions represent a common pathogenic mechanism, we assessed exon copy number by using a recently developed method, the multiplex PCR/liquid chromatography assay (MP/LC). Multiple exons were amplified using unlabeled primers, then separated by ion-pair reversed-phase high-performance liquid chromatography, and quantitated by fluorescence detection using a post-column intercalation dye under the premise that the relative peak intensities for each target directly reflect exon copy number. By using MP/LC, we identified one CHARGE syndrome patient who had a de novo deletion encompassing exons 8–12 among 13 classic CHARGE patients in whom screening by denaturing high-performance liquid chromatography (DHPLC) failed to identify point mutations and small insertions/deletions in *CHD7*. This is the first CHARGE patient who was documented to have exonic deletion of *CHD7*. The deletion closely recapitulated the *Alu*-mediated inactivation of the human *CMP-N-acetylneuraminic acid hydroxylase* gene (CMP-Neu5Ac hydroxylase), which is regarded as a novel molecular mechanism in the evolution from non-human primates to humans. As demonstrated in this study, MP/LC is a promising method for characterizing exonic deletions, which are largely left unexamined in most routine mutation analysis. © 2007 Wiley-Liss, Inc.

Key words: CHARGE syndrome; DHPLC; rearrangement; quantitative PCR

How to cite this article: Udaka T, Okamoto N, Aramaki M, Torii C, Kosaki R, Hosokai N, Hayakawa T, Takahata N, Takahashi T, Kosaki K. 2007. An *Alu* retrotransposition-mediated deletion of *CHD7* in a patient with CHARGE syndrome. Am J Med Genet Part A 143A:721–726.

INTRODUCTION

CHARGE syndrome (OMIM 214800) represents a constellation of malformations: C—coloboma of the iris or retina, H—heart defects, A—atresia of the choanae, R—retardation of growth and/or development, G—genital anomalies, and E—ear abnormalities. Heterozygous mutations in the gene encoding the *chromodomain helicase DNA-binding protein 7* (*CHD7*) on chromosome 8q12.1 were identified in

This article contains supplementary material, which may be viewed at the American Journal of Medical Genetics website at http://www.interscience.wiley.com/jpages/1552-4825/suppmat/index.html.

Grant sponsor: The Ministry of Health, Labour, and Welfare of Japan.

*Correspondence to: Kenjiro Kosaki, M.D., Division of Medical Genetics, Department of Pediatrics, Keio University School of Medicine, 35 Shinanomachi, Shinjuku-ku, Tokyo 160-8582, Japan.
E-mail: kkosaki@sc.itc.keio.ac.jp

DOI 10.1002/ajmg.a.31441

2004 as the causative gene mutations [Vissers et al., 2004]. Since then, three mutation analyses of this locus have been reported [Jongmans et al., 2006; Lalani et al., 2006; Sanlaville et al., 2006]. Among 227 patients reported in those three studies, *CHD7* mutations accounted for about 60–65% of CHARGE cases. Pathogenic mechanisms in the remaining mutation-negative cases are yet to be delineated. Possible mechanisms include whole gene deletions or exonic deletions, considering that previous studies were based mainly on PCR-sequencing that does not allow detection of these classes of mutations. Whole gene deletions do not seem to represent a prevalent mechanism because screening using multiplex ligation-dependent probe amplification (MLPA) [Jongmans et al., 2006] or fluorescence in situ hybridization (FISH) analysis with bacterial artificial chromosome (BAC) probes [Lalani et al., 2006] did not identify this class of mutations. Jongmans et al. [2006] also screened for a subset of exons (exons 2–11 and exons 33–38) using MLPA but did not identify any deletions in these regions.

To test whether exonic deletions represent a common pathogenic mechanism, we assessed exon copy numbers using a recently developed method, the multiplex PCR/liquid chromatography assay (MP/LC) [Dehainault et al., 2004]. First, a multiplex PCR with unlabeled primers enables simultaneous amplification of a subset of exons under semiquantitative conditions. We selected exons so that the subregions of the *CHD7* locus would be screened at roughly equal intervals. Second, PCR products are separated by non-denaturing ion-pair reversed-phase high performance liquid chromatography and, lastly, are quantitated by fluorescent detection using a post-column intercalation dye. The relative peak intensities for each target directly reflect exon copy number.

Thirteen classic CHARGE patients in whom screening by denaturing high-performance liquid chromatography (DHPLC) had failed to identify point mutations and small insertions/deletions in *CHD7* were screened. These patients had been enrolled in an ongoing comprehensive study that currently involves 38 patients with classic CHARGE syndrome. The enrollment criteria and a summary of the genotype–phenotype correlations in a subset of these patients (24 patients, including the one described below) have been published elsewhere [Kosaki et al., 2005; Aramaki et al., 2006]. Using MP/LC, we identified one CHARGE syndrome patient who had a de novo deletion encompassing exons 8–12.

CLINICAL REPORT

A Japanese girl was born at 34 weeks of gestation with a birth weight of 2.07 kg and a length of 43 cm to nonconsanguineous and phenotypically normal parents. At birth, she was noted to have external ear defects, coloboma of the retina and optic nerve (bilateral), labial hypoplasia, and laryngomalacia. She had neither choanal atresia nor cleft palate. She had feeding difficulties and showed failure to thrive. Nasal tube feeding was necessary until age 3 years. At age 4 months, she was noted to have bilateral hearing loss (>90 dB) and left facial nerve palsy. Ultrasonography of the heart detected no structural abnormalities. She suffered from infantile spasms (West syndrome). ACTH therapy was successful. At age 13 years, her weight was 16.2 kg (−3.6 SD) and height 113 cm (−7.2 SD). She had a square and asymmetric face. Development was severely delayed with a developmental quotient of less than 20. The severe delay may be attributable to West syndrome. She spoke no meaningful words. She could not sit without support. The patient's chromosomes were 46,XX. Neuroradiological studies revealed mild cerebral atrophy with enlarged lateral ventricles with an irregular ventricular wall. The clivus was hypoplastic. The CT scan of temporal bones revealed that semicircular canals and acoustic nerves were hypoplastic bilaterally. Arhinencephaly was not present. Serum luteinizing hormone, follicle stimulating hormone, and estradiol were undetectable at 13 years of age. The patient met both Blake and Verloes' criteria and a diagnosis of CHARGE syndrome was made [Blake et al., 1998; Verloes, 2005].

MOLECULAR AND CYTOGENETIC INVESTIGATION

DHPLC Screening

The patient was enrolled in this study after her parents provided written informed consent, according to a protocol approved by our institution's review board. Genomic DNA was isolated using a desalting column (Qiagen, Valencia, CA). The quantity of DNA in each sample was determined using a Nanodrop ND-1000 spectrophotometer (NanoDrop Technologies, Wilmington, DE). Screening for point mutations and small insertions/deletions in *CHD7* using DHPLC revealed no mutations, as described elsewhere [Kosaki et al., 2005; Aramaki et al., 2006].

Copy Number Scanning Using MP/LC Assay

We assessed exon copy numbers using a recently developed method, the MP/LC assay [Dehainault et al., 2004]. Duplex PCR was performed with 30 ng aliquots of genomic DNA. A subset of coding exons (exons 2, 5, 10, 11, 15, 18, 22, 25, 27, 28, 30, 33, and 38) of the *CHD7* gene (see the online Table I at http://www.interscience.wiley.com/jpages/1552-4825/suppmat/index.html) were amplified in duplex PCR with reference primer set *NIPBL*-exon16 (5′-cctccatagctcaaagggaat-3′ and 5′-aaacaatagagaagtgg-gggact-3′) that anneals to a locus on a chromosome

other than chromosome 8 on which *CHD7* resides. The PCRs were performed in a volume of 20 μl containing 30 ng of genomic DNA, 10 pmol of *CHD7*-forward and -reverse primer, 10 pmol of *NIPBL* exon16-forward and -reverse primer, 0.2 mM dNTPs, 1.5 mM $MgCl_2$, 5% dimethyl sulfoxide (DMSO), 0.5 U of AmpliTaq Gold polymerase, and the buffer supplied by the manufacturer (Applied Biosystems, Foster City, CA).

Aliquots of 5 μl of duplex PCR products were injected on a semi-automated Wave 3500 HT system (Transgenomic, Omaha, NE), incorporating a HSD (high sensitivity detector). HSD uses post-column intercalation chemistries, that is, SYBR Green 1 (Invitrogen, Carlsbad, CA) and fluorescence detection to provide sensitivity enhancement for the detection of DNA. Separation was performed using a DNAsep cartridge (Transgenomic) and a constant oven temperature of 50°C to ensure non-denaturing conditions. An elution gradient was generated as shown in Table I (see the online Table I at http://www.interscience.wiley.com/jpages/1552-4825/suppmat/index.html). Following separation eluted PCR products were mixed with the Wave HS Staining Solution I that contained SYBR Green 1 by using the HSX accessory, and were then detected with the FDX fluorescence detector (Transgenomic). Data were analyzed using Navigator 1.5.3 software (Transgenomic). Briefly, chromatograms from patients were first superimposed onto those of several normal controls. The fluorescence intensities were normalized by adjusting the reference peak that was obtained from the normal control with that of patients to the same height. The yield of each amplicon in the various samples was evaluated and deletion was revealed by a twofold decrease in the corresponding peak.

Initial screening (i.e., exons 2, 5, 10, 11, 15, 18, 22, 25, 27, 28, 30, 33, and 38) revealed exons 10 and 11 to be deleted, while exons 5 and 15 were not. We then performed the second round of analysis using the primer sequences of *CHD7* exons 7–13 (see the online Table I at http://www.interscience.wiley.com/jpages/1552-4825/suppmat/index.html). We found that the region spanning exons 8–12 was deleted and that two breakpoints were located within intron 7 and intron 12 (Figs. 1 and 2).

FISH Analysis

To confirm the presence of the deletion spanning exon 8–12, FISH analysis was carried out using a 5.7 kb-probe CHD7_9_12 prepared by long-range PCR using primer sets *CHD7*_FISH_1F (5′-ttgcctgt-gtccctttatcc-3′, within intron 8) and *CHD7*_FISH_1R (5′-ccgacgactagcttgactcc-3′, within exon 12) from genomic DNA of a normal control individual. The CHD7_9_12 probe hybridized to only one of the two homologous chromosome 8 regions (Fig. 3).

Breakpoint Cloning

To define the deletion more precisely, we performed long-range PCR using the exon 7 (Table I,

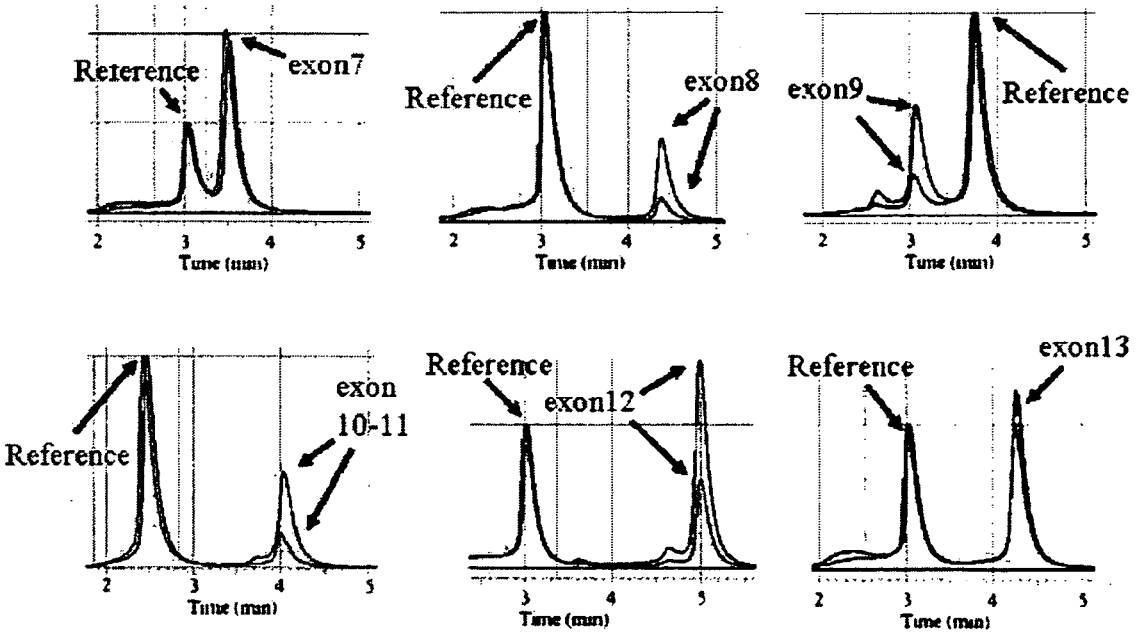

FIG. 1. MP/LC chromatograms for the six different duplexes from *CHD7* exon 7 to exon 13. x-axis: retention time in min; y-axis: fluorescence intensity. Exons under study are indicated by arrows at the tops of the corresponding peaks. The chromatograms in black and red represent the normal control and the patient, respectively. Profiles are superimposed and then normalized using the reference amplicon (*NIPBL* gene exon 16 on chromosome 5). Deleted exons are shown by two arrows comparing the normal with the patient.

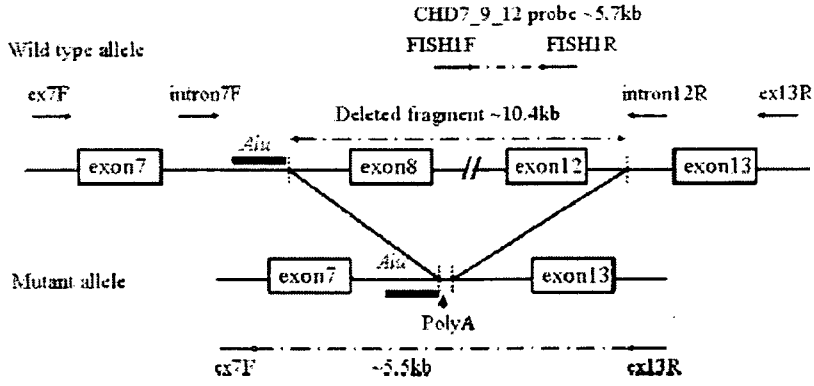

FIG. 2. Deletion of exons 8–12 of *CHD7* gene. PCR strategy for the amplification of the deleted allele. *CHD7* exons 7–13 (not drawn to scale) are boxed and numbered, introns are indicated by solid lines. F and R indicate forward and reverse primers, respectively.

EX7F (see the online Table I at http://www.interscience.wiley.com/jpages/1552-4825/suppmat/index.html)) and exon 13 (Table I, EX13R (see the online Table I at http://www.interscience.wiley.com/jpages/1552-4825/suppmat/index.html)) (Fig. 2). The long-range PCR was performed in a standard manner [Cheng et al., 1994]. Then, PCR products were analyzed by 1% agarose gel electrophoresis (Fig. 4A). In the patient specimen, a 5.5 kb PCR fragment was generated by primers EX7F and EX13R which are 16 kb apart on the wild-type allele. We concluded that the deletion spans ~10.5 kb. The deletion is predicted to cause a frameshift mutation, and a stop codon is created three codons after codon 833 (the last codon of exon 7). Sequencing of the breakpoint-spanning PCR amplicon amplified from the patients' genomic DNA provided for complete characterization of the breakpoint (Figs. 2 and 4). The sequence-verification primers were *CHD7* exon7F, exon13R, intron7F (5′-aatttttggccaggcacag-3′), and intron12R (5′-tcacacattcacgtaggacaga-3′) primers (location shown in Fig. 2).

The deletion involves 10,417 bp from intron 7 (IVS7 + 4391) to intron 12 (IVS12 + 333) and results in loss of exons 8 through 12. There was an insertion involving a poly adenine tract of approximately 100 bases at the breakpoint. The *Alu* sequence present at the 5′ end of the deleted region in the patient, which we have arbitrarily referred to as *AluΔ5*, was distinctively different from the *Alu* sequence present at the 5′ end of the parental (i.e., wild-type) genome sequence of the *AluSg* class (Fig. 5). Sequence differences between *AluΔ5* and the wild-type genome sequence were clustered within a 75 bp region at the 3′ end (see the online Fig. 6 at http://www.interscience.wiley.com/jpages/1552-4825/suppmat/index.html). The 75 bp sequence completely matched the *AluYa5/AluYa8* consensus sequence as well as at least 120 other loci within the human genome. The remaining 213 bp at the 5′ end of the *Alu* sequence of the patient completely matched the wild-type genome *AluSg* sequence. Analyses of the parents' genomic DNA revealed that the mutation occurred de novo, and neither of the parents carried the *AluΔ5* sequence.

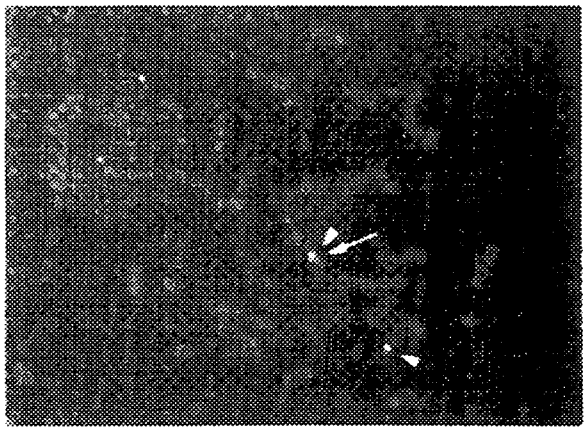

FIG. 3. Fluorescence in situ hybridization analysis of the deletion. Metaphase spreads of the patient revealed a deletion in one of the chromosome 8 homologs when hybridized with a probe prepared by long-range PCR of *CHD7* exons 9–12 from a normal control individual (red signals, arrow) and chromosome 8 centromere probes (green signals, arrowheads).

DISCUSSION

Herein, we documented a CHARGE syndrome patient who had a de novo heterozygous *Alu*-poly(A) tail-related 10.4 kb deletion of *CHD7* exons 8–12. The normal amino acid sequence would stop at residue 836 provided that transcripts from the mutant allele were stable and spliced according to the remaining exons. The truncated protein would lack functionally important domains including the chromo domain, SNF2 domain, and helicase domains. This is the first CHARGE patient who was documented to have exonic deletion of *CHD7*. The frequency of exonic deletions was 7.6% (1/13) among a set of 13 patients with CHARGE syndrome and without point mutations. Since the genomic

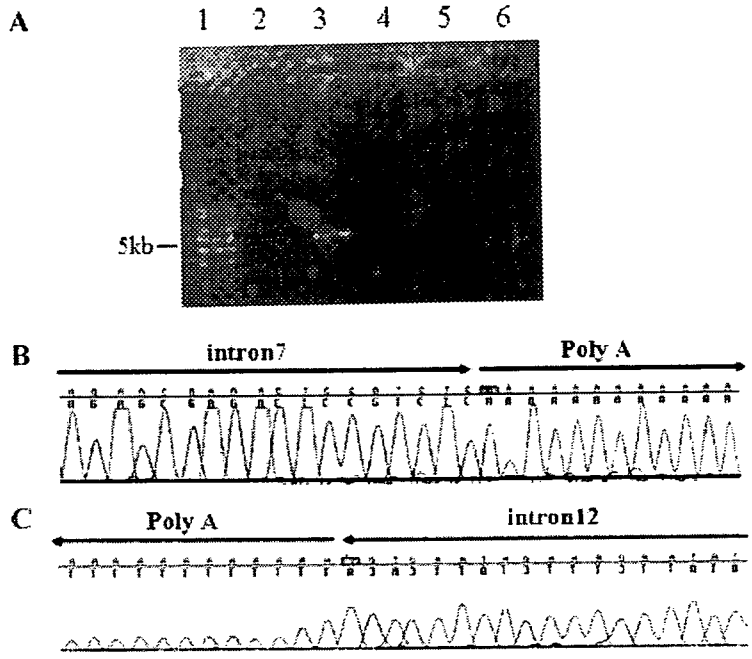

FIG. 4. **A**: Long-range PCR using primers exon7F and exon13R in Figure 2: 1 kb ladder (**lane 1**), normal control (**lane 2**), patient (**lane 3**), father of patient (**lane 4**), mother of patient (**lane 5**), and negative control (**lane 6**). A 5.5 kb product was observed for the patient's mutant allele (lane 3). No product was amplified from normal control, father of patient, or mother of patient because primers exon7F and exon13R are too far apart (16 kb) in the wild-type allele (lanes 2, 4, and 5). **B** and **C**: Sequencing across the breakpoints using the 5.5 kb long-range PCR product, and the intron7F (B) and intron12R (C: primers). Sequence direction is indicated by arrows. The poly(A) stretch can be seen after the intron sequence.

DNA samples obtained from the patients were limited, we scanned only a subset of exons during the initial screening (i.e., exons 2, 5, 10, 11, 15, 18, 22, 25, 27, 28, 30, 33, and 38); a complete screening covering all the exons might actually increase the above-mentioned frequency.

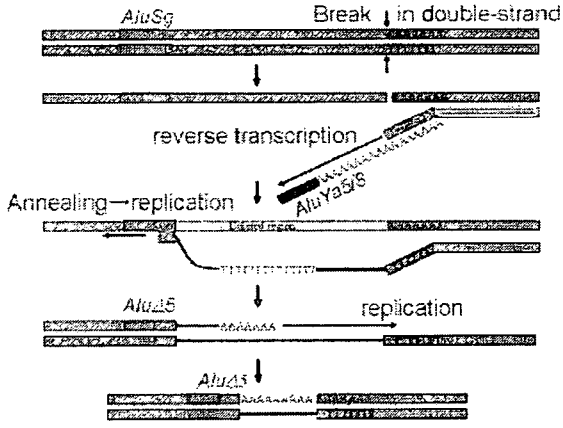

FIG. 5. Model of the *Alu*-mediated replacement event that occurred in the *CHD7* gene. The deletion was accompanied with the following phenomena: first, a poly(A) stretch of about 100 bases was inserted at the priming site. Second, about 75 bp at the 3′ end of the genomic *Alu* sequence in the wild-type allele (AluSg) were replaced by another *Alu* sequence (*AluYa5/8*) in the mutant allele. The proposed mechanism for the deletion is a double-strand break, target-priming by the free *AluYa5/8* poly(A) RNA transcript, and target-primed reverse transcription and annealing between the *AluYa5/8* cDNA and genomic *AluSg*, leading to the production of a mutant allele in which the region between the target priming site and the 3′ end of the genomic *AluSg* sequence. The resulting chimeric *Alu* sequence is designated as *AluΔ5*. The possible reason why only the 3′ end of the *AluSg* sequence was replaced is discussed in the text.

The deletion in the patient closely recapitulated the *Alu*-mediated inactivation of the human *CMP-N-acetylneuraminic acid hydroxylase* gene (CMP-Neu5Ac hydroxylase), which is regarded as a novel molecular mechanism in the evolution from non-human primates to humans [Hayakawa et al., 2001]. The proposed mechanism for *CMP-Neu5Ac hydroxylase* gene inactivation is a double-strand break, target-priming by the free *Alu* poly(A) RNA transcript, and target-primed reverse transcription and annealing between the *Alu* cDNA and genomic *Alu*, leading to the production of a mutant allele in which the region between the target priming site and the genomic *Alu* sequence has been deleted. The same mechanism would explain the characteristic features of the genomic sequence of the deleted mutant allele in the patient: first, a poly(A) stretch of about 100 bases was inserted at the priming site. The poly(A) was most likely derived from a free Alu RNA transcript. Second, about 75 bp at the 3′ end of the genomic *Alu* sequence in the wild-type allele (*AluSg*) were replaced by another *Alu* sequence (*AluYa5/8*) in the mutant allele. The reason why only the 3′ end of the *AluSg* sequence was replaced is unclear. Reverse transcription from the free *AluYa5/8* poly(A) RNA may have been prematurely terminated; alternatively, the free *AluYa5/8* poly(A) RNA may have been shortened as a result of degradation prior to reverse transcription.

Deletion associated with an *Alu*-poly(A) tail was previously reported in a breast cancer family with the *BRCA2* mutation [Wang et al., 2001]. In the BRCA2 mutation, 60 adenines were inserted at the deletion junction, suggesting target-priming by the free *Alu* poly(A) RNA transcript followed by target-primed reverse transcription as the mechanistic basis of the rearrangements.

The patient was identified among 13 classic CHARGE patients in whom DHPLC screening failed to identify point mutations, small deletions, or insertions in *CHD7*. Hence, exonic deletions of *CHD7* may not be so common among patients with CHARGE syndrome. Nevertheless, development of an assay system to detect this class of mutations is critical because actual prevalence of such mutations will never be appreciated until they have been surveyed appropriately. Recently, Douglas et al. [2005] screened for exonic deletions in 18 classic Sotos syndrome cases in which *NSD1* point mutations and small insertion/deletions and 5q35 microdeletions were excluded. They identified eight cases with exonic deletions, highlighting the clinical importance of this class of mutations.

In the *NSD1* partial deletion study by Douglas et al. [2005], MLPA [Sellner and Taylor, 2004] was applied to achieve relative quantification of individual exons. In MLPA, two adjacently hybridized probes are ligated and then PCR amplified using fluorescent labeled universal primers that correspond to sequence tags present in every probe. Each probe is designed to give a uniquely sized product resulting in a ladder of amplified products that can be quantified by fluorescent electrophoretic analysis. Unfortunately, development of such kits in laboratories other than those dedicated to MLPA technology would be time-consuming and difficult to implement [Sellner and Taylor, 2004]. As demonstrated in this study, MP/LC is a promising alternative to MLPA in characterizing a broad spectrum of deletions in various multiple malformation syndromes as MP/LC is largely independent of the genomic locus and easy to handle.

REFERENCES

Aramaki M, Udaka T, Kosaki R, Makita Y, Okamoto N, Yoshihashi H, Oki H, Nanao K, Moriyama N, Oku S, Hasegawa T, Takahashi T, Fukushima Y, Kawame H, Kosaki K. 2006. Phenotypic spectrum of CHARGE syndrome with CHD7 mutations. J Pediatr 148:410–414.

Blake KD, Davenport SL, Hall BD, Hefner MA, Pagon RA, Williams MS, Lin AE, Graham JM Jr. 1998. CHARGE association: An update and review for the primary pediatrician. Clin Pediatr 37:159–173.

Cheng S, Fockler C, Barnes WM, Higuchi R. 1994. Effective amplification of long targets from cloned inserts and human genomic DNA. Proc Natl Acad Sci USA 91:5695–5699.

Dehainault C, Lauge A, Caux-Moncoutier V, Pages-Berhouet S, Doz F, Desjardins L, Couturier J, Gauthier-Villars M, Stoppa-Lyonnet D, Houdayer C. 2004. Multiplex PCR/liquid chromatography assay for detection of gene rearrangements: Application to RB1 gene. Nucleic Acids Res 32:e139.

Douglas J, Tatton-Brown K, Coleman K, Guerrero S, Berg J, Cole TR, Fitzpatrick D, Gillerot Y, Hughes HE, Pilz D, Raymond FL, Temple IK, Irrthum A, Schouten JP, Rahman N. 2005. Partial NSD1 deletions cause 5% of Sotos syndrome and are readily identifiable by multiplex ligation dependent probe amplification. J Med Genet 42:e56.

Hayakawa T, Satta Y, Gagneux P, Varki A, Takahata N. 2001. Alu-mediated inactivation of the human CMP-N-acetylneuraminic acid hydroxylase gene. Proc Natl Acad Sci USA 98:11399–11404.

Jongmans MC, Admiraal RJ, van der Donk KP, Vissers LE, Baas AF, Kapusta L, van Hagen JM, Donnai D, de Ravel TJ, Veltman JA, Geurts van Kessel A, De Vries BB, Brunner HG, Hoefsloot LH, van Ravenswaaij CM. 2006. CHARGE syndrome: The phenotypic spectrum of mutations in the CHD7 gene. J Med Genet 43:306–314.

Kosaki K, Udaka T, Okuyama T. 2005. DHPLC in clinical molecular diagnostic services. Mol Genet Metab 86:117–123.

Lalani SR, Safiullah AM, Fernbach SD, Harutyunyan KG, Thaller C, Peterson LE, McPherson JD, Gibbs RA, White LD, Hefner M, Davenport SL, Graham JM, Bacino CA, Glass NL, Towbin JA, Craigen WJ, Neish SR, Lin AE, Belmont JW. 2006. Spectrum of CHD7 mutations in 110 individuals with CHARGE syndrome and genotype–phenotype correlation. Am J Hum Genet 78:303–314.

Sanlaville D, Etcheverís HC, Gonzales M, Martinovic J, Clement-Ziza M, Delezoide AL, Aubry MC, Pelet A, Chemouny S, Cruaud C, Audollent S, Esculpavit C, Goudefroye G, Ozilou C, Fredouille C, Joye N, Morichon-Delvallez N, Dumez Y, Weissenbach J, Munnich A, Amiel J, Encha-Razavi F, Lyonnet S, Vekemans M, Attie-Bitach T. 2006. Phenotypic spectrum of CHARGE syndrome in fetuses with CHD7 truncating mutations correlates with expression during human development. J Med Genet 43:211–317.

Sellner LN, Taylor GR. 2004. MLPA and MAPH: New techniques for detection of gene deletions. Hum Mutat 23:413–419.

Verloes A. 2005. Updated diagnostic criteria for CHARGE syndrome. Am J Med Genet Part A 133A:306–308.

Vissers LE, van Ravenswaaij CM, Admiraal R, Hurst JA, de Vries BB, Janssen IM, van der Vliet WA, Huys EH, de Jong PJ, Hamel BC, Schoenmakers EF, Brunner HG, Veltman JA, van Kessel AG. 2004. Mutations in a new member of the chromodomain gene family cause CHARGE syndrome. Nat Genet 36:955–957.

Wang T, Lerer I, Gueta Z, Sagi M, Kadouri L, Peretz T, Abeliovich D. 2001. A deletion/insertion mutation in the BRCA2 gene in a breast cancer family: A possible role of the Alu-polyA tail in the evolution of the deletion. Genes Chromosomes Cancer 31:91–95.

American Journal of Medical Genetics Part A 143A:768–769 (2007)

Research Letter

Monozygotic Twins of Smith–Magenis Syndrome

Rika Kosaki,[1]* Torayuki Okuyama,[1] Toju Tanaka,[1] Ohsuke Migita,[1] and Kenjiro Kosaki[2]

[1]Department of Clinical Genetics and Molecular Medicine, National Center for Child Health and Development. Tokyo, Japan
[2]Department of Pediatrics, Keio University School of Medicine, Tokyo, Japan

Received 2 July 2006; Accepted 25 November 2006

How to cite this article: Kosaki R, Okuyama T, Tanaka T, Migita O, Kosaki K. 2007. Monozygotic twins of Smith–Magenis syndrome. Am J Med Genet Part A 143A:768–769.

To the Editor:

Smith–Magenis syndrome (SMS) is caused by an interstitial deletion of chromosome 17p11.2 [Greenberg et al., 1991] involving the *RAI1*gene. Characteristic features include a broad squared face, midface hypoplasia, mild upslanting palpebral fissures, prognathism, upper lip eversion [Allanson et al., 1999], a short stature, moderate mental retardation, sleep disturbances [Smith et al., 1998b], and behavioral problems, such as self-injury [Smith et al., 1998a]. Among more than 150 cases of SMS reported to date, all the cases have been sporadic except for one family in which the unaffected mothers were mosaic for a 17p11.2 deletion. Sib pairs or twin pairs have not been reported [Zori et al., 1993]. Here, we document the first reported case of monozygotic twins with SMS.

The male twins were born to a 26-year-old Japanese G2P1-3 woman with no previous medical problems. Consanguinity or a family history of mental retardation was not present. The pregnancy was unremarkable, and the twins were delivered at 37 weeks of gestation. The placentation was diamniotic and monochorionic. At birth, the weight of twin A was 1,812 g, his length was 42.5 cm, and his head circumference was 31.1 cm. His Apgar score was 5–7. A head CT revealed Dandy–Walker variant-type cerebellar hypoplasia. The birth weight of twin B was 2,564 g, his length was 46 cm, and his head circumference was 32 cm. The postnatal courses of the twins were comparable. They sat alone at 10 months, walked alone at 14 months, and spoke their first words at 24 months. Both twins had recurrent episodes of bronchitis and otitis media requiring tympanostomy tube replacements. At the age of 3 years, the twins were referred to our genetic department because of developmental delays and self-injuring activities such as skin picking and nail yanking (onychotillomania). Dysmorphic features, which were all concordant between the twins, included an everted upper lip with tented appearance micrognathia, a broad square-shaped face, close-spaced eyes, and short broad hands (Fig. 1). At 5 years of age, the twins developed sleep disturbances. At the age of 5 years and 5 months, the weight of twin A was 17.0 kg (−0.63 SD), his length was 102.2 cm (−1.7 SD), and his head circumference was 49.0 cm (−1.6 SD). At the same age, the weight of twin B was 21.25 kg (+0.76 SD), his length was 106.4 cm (−0.8 SD), and his head circumference was 52 cm (+0.5 SD). The intelligent quotients of twin A and twin B on the Tanaka–Binet scale were 44 and 53, respectively. Karyotyping

FIG. 1. Facial features of monozygotic twins with Smith–Magenis syndrome (right: Twin A; left: Twin B).

Grant sponsor: The Ministry of Health, Labour, and Welfare of Japan.

*Correspondence to: Rika Kosaki, M.D., Department of Clinical Genetics and Molecular Medicine, National Center for Child Health and Development, 2-10-1 Okura, Setagaya-ku, Tokyo 157-8535, Japan.
E-mail: kosaki-r@ncchd.go.jp

DOI 10.1002/ajmg.a.31647

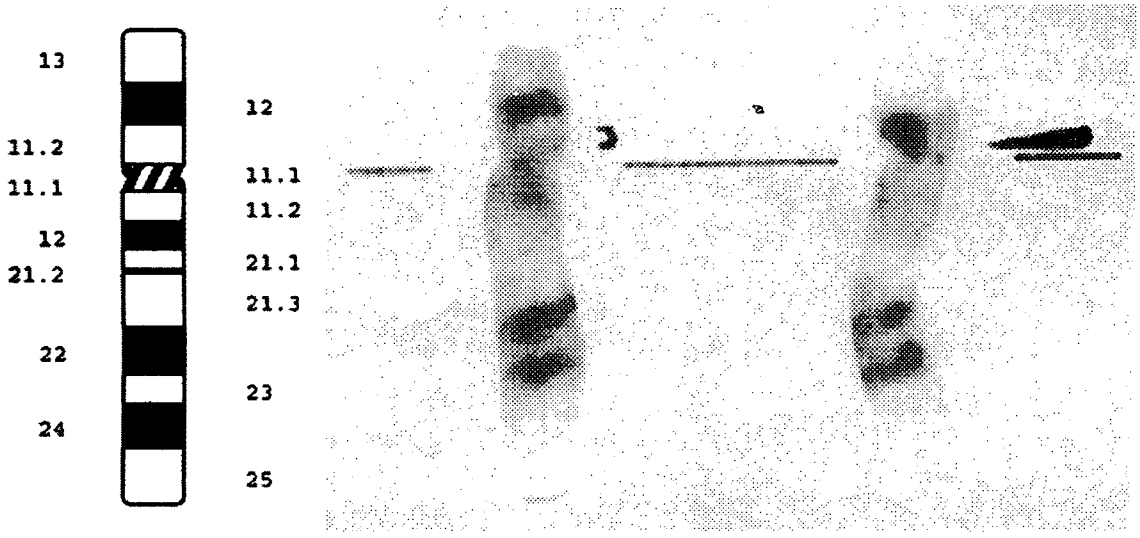

FIG. 2. Partial karyotype of chromosome 17 from twin A.

(Fig. 2) revealed a deletion of (17)(p11.2p11.2). The parental karyotypes were unavailable. The Smith–Magenis region-specific FISH probe (Vysis) hybridized to only one of the two homologous chromosome 17 regions, allowing us to assign the twins' karyotype as 46,XY. ish del(17)(p11.2p11.2) (SHMT1/TOP3/FLII/LLGL1-).

Identical twins have been reported in several multiple congenital anomaly syndromes including Crouzon syndrome [Lajeunie et al., 2000], Alagille syndrome [Kamath et al., 2002], Sotos syndrome [Brown et al., 1998], and 22q11.2 deletion syndrome [Goodship et al., 1995]. The discordance in the severities of the twin pairs in these previous reports point towards a significant role of chance-like variations in the pathogenetic actions of the mutated genes. In contrast, the SMS twins reported herein demonstrated strikingly similar developmental and behavior patterns. This observation does not necessarily indicate but does suggest a relatively large contribution of genetic factors in the evolution of the SMS phenotype.

REFERENCES

Allanson JE, Greenberg F, Smith AC. 1999. The face of Smith–Magenis syndrome: A subjective and objective study. J Med Genet 36:394–397.

Brown WT, Wisniewski KE, Sudhalter V, Keogh M, Tsiouris J, Miezejeski C, Schaefer GB. 1998. Identical twins discordant for Sotos syndrome. Am J Med Genet 79:329–333.

Goodship J, Cross I, Scambler P, Burn J. 1995. Monozygotic twins with chromosome 22q11 deletion and discordant phenotype. J Med Genet 32:746–748.

Greenberg F, Guzzetta V, Montes de Oca-Luna R, Magenis RE, Smith AC, Richter SF, Kondo I, Dobyns WB, Patel PI, Lupski JR. 1991. Molecular analysis of the Smith–Magenis syndrome: A possible contiguous-gene syndrome associated with del(17)(p11.2). Am J Hum Genet 49:1207–1218.

Kamath BM, Krantz ID, Spinner NB, Heubi JE, Piccoli DA. 2002. Monozygotic twins with a severe form of Alagille syndrome and phenotypic discordance. Am J Med Genet 112:194–197.

Lajeunie E, Bonaventure J, El Ghouzzi V, Catala M, Renier D. 2000. Monozygotic twins with Crouzon syndrome: Concordance for craniosynostosis and discordance for thumb duplication. Am J Med Genet 91:159–160.

Smith AC, Dykens E, Greenberg F. 1998a. Behavioral phenotype of Smith–Magenis syndrome (del 17p11.2). Am J Med Genet 81:179–185.

Smith AC, Dykens E, Greenberg F. 1998b. Sleep disturbance in Smith–Magenis syndrome (del 17 p11.2). Am J Med Genet 81:186–191.

Zori RT, Lupski JR, Heju Z, Greenberg F, Killian JM, Gray BA, Driscoll DJ, Patel PI, Zackowski JL. 1993. Clinical, cytogenetic, and molecular evidence for an infant with Smith–Magenis syndrome born from a mother having a mosaic 17p11.2p12 deletion. Am J Med Genet 47:504–511.

American Journal of Medical Genetics Part A 143A:1087–1090 (2007)

Clinical Report

Wide Phenotypic Variations Within a Family With *SALL1* Mutations: Isolated External Ear Abnormalities to Goldenhar Syndrome

Rika Kosaki,[1] Rika Fujimaru,[2] Hazuki Samejima,[3] Hiroshi Yamada,[4] Kosuke Izumi,[3] Kazumoto Iijima,[5] and Kenjiro Kosaki[3]*

[1]Department of Clinical and Molecular Genetics, National Center for Child Health and Development, Tokyo, Japan
[2]Department of Pediatrics, Osaka City Kita Hospital, Osaka, Japan
[3]Department of Pediatrics, Keio University, School of Medicine, Tokyo, Japan
[4]Department of Pediatrics, Osaka City General Hospital, Osaka, Japan
[5]Department of Nephrology, National Center for Child Health and Development, Tokyo, Japan

Received 13 September 2006; Accepted 30 December 2006

We report on wide phenotypic variations within a family with *SALL1* mutations; the elder sister presented with a Townes–Brocks syndrome phenotype including external ear anomalies, preaxial polydactyly, and anteriorly placed anus, whereas the younger sister presented with a phenotype resembling Goldenhar syndrome, including atretic ear canals, mandibular hypoplasia, and right preaxial polydactyly as well as an epibulbar dermoid. The mother had abnormal external ears but was otherwise structurally normal, and the father was asymptomatic. Analysis of the *SALL1* gene revealed that both daughters were heterozygous for nonsense mutation 1256T>A (L419X), that is present 5' to the region encoding the first double zinc finger. The mother was heterozygous for the L419X mutation. The younger daughter is the first patient with a *SALL1* mutation to exhibit a classic Goldenhar syndrome-like phenotype with an epibulbar dermoid. The observation lends further support to the concept that Goldenhar syndrome is an etiologically heterogeneous disorder that may have a genetic basis in some cases. © 2007 Wiley-Liss, Inc.

Key words: Townes–Brocks syndrome; Goldenhar syndrome; epibulbar dermoid; *SALL1*

How to cite this article: Kosaki R, Fujimaru R, Samejima H, Yamada H, Izumi K, Iijima K, Kosaki K. 2007. Wide phenotypic variations within a family with *SALL1* mutations: Isolated external ear abnormalities to Goldenhar syndrome. Am J Med Genet Part A 143A:1087–1090.

INTRODUCTION

Townes–Brocks syndrome (TBS) [Townes and Brocks, 1972] is characterized by first and second arch defects including the ears and jaw, kidney malformations, preaxial defects of the limbs, and anal defects. Hemifacial microsomia (HFM) is characterized by first and second arch defects including the ears and jaw and is sometimes associated with preaxial defects of the upper limbs and kidney malformations. HFM patients exhibiting epibulbar dermoid are diagnosed as having Goldenhar syndrome (GS) [Goldenhar, 1952]. TBS and HFM/GS have a significant number of overlapping features, including first and second arch defects, preaxial defects of the upper limb, and kidney malformations.

TBS is an autosomal dominant condition caused by mutations in the *SALL1* gene [Kohlhase et al., 1998], and many familial cases have been reported [Kohlhase et al., 1999]. Meanwhile, most cases of GS and HFM occur sporadically, and the pathological basis of GS is not well established [Rollnick and Kaye, 1983]. Discordance in monozygotic twins with GS/HFM [Schinzel et al., 1979; Boles et al., 1987] suggests an environmental or multifactorial etiology rather than a simple genetic cause. However, exceptional familial cases [Stoll et al., 1998] and those with chromosomal abnormalities [Josifova et al., 2004]

Grant sponsor: The Ministry of Health, Labour, and Welfare of Japan.
*Correspondence to: Kenjiro Kosaki, M.D., Department of Pediatrics, Keio University School of Medicine, 35 Shinanomachi, Shinjuku-ku, Tokyo 160-8582, Japan. E-mail: kkosaki@sc.itc.keio.ac.jp
DOI 10.1002/ajmg.a.31700

suggest that some, if not all, GS and HFM cases may have a genetic etiology.

Several authors have documented patients with intermediate phenotypes between TBS and GS/HFM: In some families, affected subjects show features typical of both TBS and GS/HFM [Moeschler and Clarren, 1982; Gabrielli et al., 1993; Johnson et al., 1996]. Kohlhase et al. [1999] performed a mutation analysis for *SALL1* in a patient with an HFM phenotype who had been originally reported by Gabrielli et al. and identified a *SALL1* mutation. Because the patient did not have epibulbar dermoid, whether the GS phenotype (i.e., HFM with epibulbar dermoid) can be caused by a *SALL1* mutation has yet to be determined.

CLINICAL REPORT

Patient 1

Patient 1 was a 5-year-old girl who had been born after 39 weeks of gestation to a 32-year-old gravida 2 para 0 woman with abnormal external ears. The 37-year-old father was normal from a structural standpoint. The patient was delivered vaginally and had a birth weight of 2,444 g (−1.5 SD).

At age 5 years, the patient's height was 103.5 cm (−2 SD) and her weight was 16.1 kg (−1.5 SD). She had overfolded superior helices (Fig. 1) with moderate sensory neural hearing impairment, preaxial polydactyl and syndactyly of the first and second toes, and an anteriorly placed anus. Sonographic studies showed hypoplastic kidneys, and she had mild azotemia, with a serum creatinine concentration of 0.75 mg/dl and a blood urea nitrogen level of 15.8 mg/dl. Her chromosomes were normal.

Patient 2

Patient 2 was the younger sister of Patient 1; she was 3 years old at the time of examination. She had been the result of an uneventful pregnancy and had been born after 39 weeks of gestation. Her birth weight was 2,649 g (−0.7 SD). Neonatal mass screening had revealed hypothyroidism, and she had been treated with thyroxine supplementation. A physical examination when she was 3 years old showed a height of 85.5 cm (−2 SD) and a weight of 11.5 kg (−1.5 SD). She had epibulbar dermoid (Fig. 2A,B) bilateral microtia with atretic ear canals (Fig. 2C), mandibular hypoplasia, and right preaxial polydactyly of the toes (Fig. 2D). She had an anteriorly placed anus. An audiological examination revealed profound hearing loss. Sonographic studies showed hypoplastic kidneys, and she had moderate azotemia, with a serum creatinine concentration of 1.05 mg/dl and a blood urea nitrogen level of 34.9 mg/dl. Her chromosomes were normal. She did not have any vertebral defects.

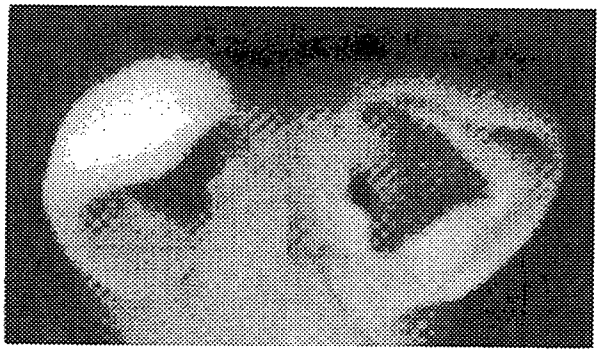

FIG. 1. Patient 1: note overfolded superior helices.

The mother had abnormal external ears comprising mild microtia but was otherwise normal. Her serum creatinine concentration was 0.9 mg/dl, and her blood urea nitrogen level was 12.2 mg/dl. The father was structurally normal; his creatinine concentration was 0.7 mg/dl, and his blood urea nitrogen level was 14.2 mg/dl.

MOLECULAR INVESTIGATIONS

Genomic DNA (the three exons and flanking introns of the *SALL1* gene) was obtained from leukocyte samples and amplified using PCR [Kohlhase et al., 1999]. The PCR products were then directly sequenced from both directions using an ABI3100 autosequencer (ABI, Foster City, CA). Both daughters were heterozygous for a nonsense mutation, 1256T>A (L419X), that is present 5' to the region encoding the first double zinc finger. The L419X mutation was predicted to cause protein truncation. The predicted truncated SALL1 protein would lack all double-zinc finger domains. In addition, both daughters were heterozygous for a single base change, 809C>T, leading to an amino acid substitution P270L that has been reported as a polymorphism [Botzenhart et al., 2005; Bohm et al., 2006]. The mother, who had dysplastic ears, was heterozygous for L419X and the asymptomatic father was heterozygous for the P270L substitution. L419X mutation has not been reported in the literature.

DISCUSSION

Here, we report on a family with *SALL1* mutations; the elder sister presented with a TBS phenotype, whereas the younger sister presented with a GS phenotype with epibulbar dermoid. The mother and her two daughters were all heterozygous for an L419X mutation in *SALL1*. Thus, a high degree of variable expressivity was observed within the family; the mother had abnormal pinnae but was otherwise asymptomatic, whereas both daughters were more severely affected and exhibited renal hypoplasia and hearing loss.

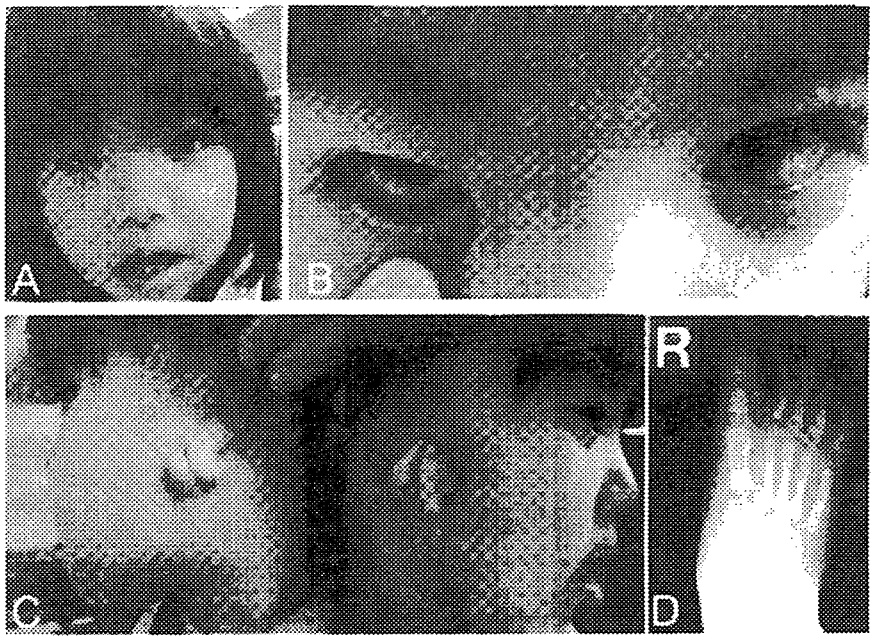

FIG. 2. Patient 2: note epibulbar dermoid (**A**,**B**), bilateral microtia with atretic ear canals (**C**), and right preaxial polydactyly of the toes (**D**).

To our knowledge, the younger daughter is the first patient with an *SALL1* mutation to exhibit an epibulbar dermoid and phenotypic features of HFM. Since an epibulbar dermoid is a hallmark of GS, this case indicates that GS can be associated with a *SALL1* mutation. Our observation is compatible with a previous report describing an affected family member with a GS-like phenotype in a three-generation TBS family [Johnson et al., 1996] that had not yet undergone genetic analysis for a *SALL1* mutation. In the past, the pathogenesis of GS has been considered to be nongenetic because multiple discordant monozygotic twin pairs with only one twin exhibiting the GS phenotype have been reported [Schinzel et al., 1979; Boles et al., 1987]. The proposed mechanisms include the vascular disruption theory, in which branchial arch defects are explained by a vascular accident in the embryonic stapedial artery [Poswillo, 1975]. The documentation of a *SALL1*-mutation positive patient exhibiting a GS phenotype lends further support to the concept that GS is an etiologically heterogeneous disorder that may have a genetic basis in some cases.

REFERENCES

Bohm J, Munk-Schulenburg S, Felscher S, Kohlhase J. 2006. SALL1 mutations in sporadic Townes-Brocks syndrome are of predominantly paternal origin without obvious paternal age effect. Am J Med Genet Part A 140A:1904–1908.

Boles DJ, Bodurtha J, Nance WE. 1987. Goldenhar complex in discordant monozygotic twins: A case report and review of the literature. Am J Med Genet 28:103–109.

Botzenhart EM, Green A, Ilyina H, Konig R, Lowry RB, Lo IF, Shohat M, Burke L, McGaughran J, Chafai R, Pierquin G, Michaelis RC, Whiteford ML, Simola KO, Rosler B, Kohlhase J. 2005. SALL1 mutation analysis in Townes-Brocks syndrome: Twelve novel mutations and expansion of the phenotype. Hum Mutat 26:282.

Gabrielli O, Bonifazi V, Offidani AM, Cellini A, Coppa GV, Giorgi PL. 1993. Description of a patient with difficult nosological classification: Goldenhar syndrome or Townes-Brocks syndrome? Minerva Pediatr 45:459–462.

Goldenhar M. 1952. Associations malformatives de l'oeil et de l'oreille: En particulier, le syndrome: Dermoide epibulbaire-appendices auriculaires–fistula auris congenita et ses relations avec la dysostose mandibulo-faciale. J Genet Hum 1: 243–282.

Johnson JP, Poskanzer LS, Sherman S. 1996. Three-generation family with resemblance to Townes-Brocks syndrome and Goldenhar/oculoauriculovertebral spectrum. Am J Med Genet 61:134–139.

Josifova DJ, Patton MA, Marks K. 2004. Oculoauriculovertebral spectrum phenotype caused by an unbalanced t(5;8) (p15.31;p23.1) rearrangement. Clin Dysmorphol 13:151–153.

Kohlhase J, Wischermann A, Reichenbach H, Froster U, Engel W. 1998. Mutations in the SALL1 putative transcription factor gene cause Townes-Brocks syndrome. Nat Genet 18: 81–83.

Kohlhase J, Taschner PE, Burfeind P, Pasche B, Newman B, Blanck C, Breuning MH, ten Kate LP, Maaswinkel-Mooy P, Mitulla B, Seidel J, Kirkpatrick SJ, Pauli RM, Wargowski DS, Devriendt K, Proesmans W, Gabrielli O, Coppa GV, Wesby-van Swaay E, Trembath RC, Schinzel AA, Reardon W, Seemanova E, Engel W. 1999. Molecular analysis of SALL1 mutations in Townes-Brocks syndrome. Am J Hum Genet 64:435–445.

Moeschler J, Clarren SK. 1982. Familial occurrence of hemifacial microsomia with radial limb defects. Am J Med Genet 12:371–375.